Infrared Laser Post-Ionization of Large Biomolecules from an IR-MALD(I) Plume

Arne Leisner, Andreas Rohlfing, Stefan Berkenkamp, Franz Hillenkamp, and Klaus Dreisewerd

Institute of Medical Physics and Biophysics, Westfälische-Wilhelms Universität, Münster, Germany

A two-infrared laser desorption/ionization method is described. A first laser, which was either an Er:YAG laser or an optical parametric oscillator (OPO), served for ablation/vaporization of small volumes of analyte/matrix sample at fluences below the ion detection threshold for direct matrix-assisted laser desorption/ionization mass spectrometry (MALDI-MS). A second IR-laser, whose beam intersected the expanding ablation plume at a variable distance and time delay, was used to generate biomolecular ions out of the matrix-assisted laser desorption (MALD) plume. Either one of the two above lasers or an Er:YSGG laser was used for post-ionization. Glycerol was used as IR-MALDI matrix, and mass spectra of peptides, proteins, as well as nucleic acids, some of which in excess of 10^5 u in molecular weight, were recorded with a time-of-flight mass spectrometer. A mass spectrum of cytochrome *c* from a water ice matrix is also presented. The MALD plume expansion was investigated by varying the position of the post-ionization laser beam above the glycerol sample surface and its delay time relative to the desorption laser. Comparison between the OPO (pulse duration, τ_L = 6 ns) and the Er:YAG laser (τ_L ~120 ns) as primary excitation laser demonstrates a significant effect of the laser pulse duration on the MALD process. (J Am Soc Mass Spectrom 2004, 15, 934–941) © 2004 American Society for Mass Spectrometry

Pulsed lasers are used for the generation of biomolecular ions in different mass spectrometric methods. In matrix-assisted laser desorption/ionization mass spectrometry (MALDI-MS) [1, 2], desorption/ionization is achieved in a complex, single-laser initiated process [3–5]. Lasers emitting in the ultraviolet (UV) [1, 2, 6] or infrared (IR) wavelength range [7, 8] are employed for MALDI. In combination with time-of-flight mass spectrometry (TOF-MS), the generation and detection of analyte ions from all classes of large biomolecules is possible with this method. For proteins, the upper limit is in the range of several hundred thousand mass units.

In resonance-enhanced multiphoton ionization (REMPI) mass spectrometry, samples are ablated/vaporized by an IR- or UV-laser and photoionized with a second, typically wavelength-tunable, UV-laser [9]. Prior to the photoionization step, analyte molecules are commonly injected into a supersonic molecular beam. The upper mass limit of the UV-REMPI-MS approach is about (2–3) $\times$ 10^3 u [10]. In some studies, the primary laser has been substituted by other means of vaporization, mostly by thermal evaporation [11, 12]. However, only inorganic and relatively small organic molecules have been found to be amenable with these latter modifications. REMPI-MS with a free electron laser emitting in the middle- to far-IR has recently been applied in spectroscopic studies of gas phase molecules and clusters (e.g., fullerenes). Resonant absorption of several ten to hundred photons with subsequent thermal electron emission was assumed as ionization pathway [13]. Results for larger biomolecules were not reported.

Another two-laser approach has recently been presented by Little et al. [14]. In this work, a 10.6 μm CO_2 laser was used to irradiate a MALDI sample at sub-ion detection threshold fluences. A second pulse of a 337 nm nitrogen laser initiated the generation of ions with adjustable delay to the IR-laser pulse. A strong delay-time dependence of the UV-MALDI ion yield was reported.

In aerosol mass spectrometry, ionization is achieved by UV-laser vaporization of single (aerosol) particles [15–18]. Mostly atoms and small inorganic molecules, or small fragments from organic molecules, are detectable with this method. The detection of peptides in the 1000 u range has been facilitated in an aerosol mass spectrometer when a MALDI matrix/analyte solution was sprayed [19]. Two studies by Thomson and Murphy [20] and Dessiaterik et al. [21] also demonstrated CO_2 laser-induced ionization of inorganic and small organic molecules from aerosols at 10.6 μm excitation wavelength.

Published online May 10, 2004

Address reprint requests to Dr. K. Dreisewerd, Institute of Medical Physics and Biophysics, University of Münster, Robert-Koch-Str. 31, D-48149 Münster, Germany. E-mail: dreisew@uni-muenster.de

1044-0305/04/$30.00
doi:10.1016/j.jasms.2004.03.010

Received January 14, 2004
Revised March 23, 2004
Accepted March 23, 2004

Pulsed IR-lasers are also used in laser-induced desorption/ionization mass spectrometry from a liquid beam (LILBID-MS [22–24]). The intact desorption/ionization of even weakly bound complexes, like holohemoglobin, was attributed to the native environment of the LILBID solvents, usually water or aqueous solutions containing methanol or ethanol, as well as to particularly soft desorption/ionization conditions. A major drawback of the liquid beam technique is the consumption of rather high amounts of analyte because only a very limited fraction of the liquid beam is sampled.

Finally, a cw-CO_2 laser has been used to promote vaporization from aqueous solutions effusing from the tip of a capillary, in a set-up otherwise similar to an electrospray ionization (ESI) ion source (laser spray, [25]).

This article presents initial results of a novel approach, in which a first IR-laser is used to vaporize small volumes of analyte/matrix mixtures in an IR-MALD process and a second IR-laser is used for infrared "post-ionization" (IRPI) of biomolecules in the expanding MALD particle plume. IRPI-MALD mass spectra of peptides, proteins, and nucleic acids, desorbed from a glycerol matrix, are presented. The generation of cytochrome *c* ions from a water ice matrix is furthermore shown. The set-up was also used to investigate the expansion dynamics of the glycerol-MALD-plume by either varying the delay time (τ_{IRPI}) between the laser pulses or the position of the IRPI laser beam relative to the primary ablation site. Primary excitation by the OPO (τ_L = 6 ns) was compared to that by the Er:YAG laser (τ_L ~120 ns).

Experimental

Time-of-Flight Mass Spectrometer

Experiments were carried out with an in-house built reflectron time-of-flight (TOF) mass spectrometer of 3.5 m equivalent flight length (Figure 1a), operated in the positive ion mode. Ions were accelerated in a two stage Wiley/McLaren ion extraction source with distances between sample plate and first grid of 6 mm, and a distance between first and second grid of 12.5 mm. Unless otherwise stated, continuous extraction conditions were applied. The electrical potential at the sample plate was set to U_{tar} = +16 kV and that of the first grid to U_{extr} = +14.5 kV, thus providing an extraction field of ~250 V mm^{-1} in the interspace. The second grid was grounded. An Einzel lens served to image the ion beam onto the detector. All measurements were performed in reflector TOF mode. A venetian-blind secondary electron multiplier (SEM; 9643/A, Emi-Thorn, Ruislip, UK), equipped with a conversion dynode (CD) mounted 10 mm in front of the first dynode of the SEM, was used for ion detection. For analytes exceeding 10^4 u in mass, a post-acceleration voltage of −20 kV was applied to the conversion dynode in order to increase the ion signal by efficient generation of secondary ions.

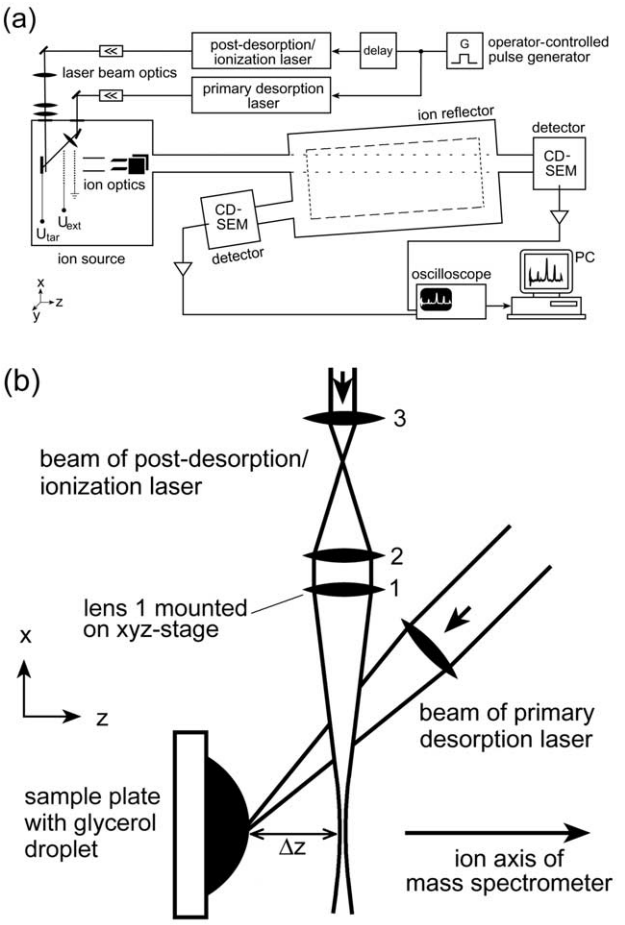

Figure 1. (**a**) The employed reflectron-TOF mass spectrometer with the primary IR-MALD and the IRPI laser beam. An xyz-micrometer translation stage was used to adjust the position of the IRPI laser beam focus relative to the primary laser spot. Ions were detected with a conversion-dynode secondary electron multiplier combination (CD-SEM). (**b**) Close-up view of the two-beam set-up. Δz represents the axial distance between the apex of the glycerol drop and the "edge" of the IRPI laser beam.

For smaller ions, a low potential difference between conversion dynode and SEM of a few hundred volts was used. In this "electron-only mode", only secondary electrons are amplified. Ion signals were recorded with a digital oscilloscope (LeCroy 9354A, Chestnut Ridge, NY) and then transferred to a PC. The sample plate was visualized with a CCD camera at an optical resolution of ~20 μm. The residual pressure in the sample chamber of the mass spectrometer was ~5×10^{-7} mbar.

The instrument was equipped with four different IR-lasers: An Er:YAG laser (Speser, Spektrum GmbH, Berlin, Germany) with an emission wavelength λ of 2.94 μm (pulse duration, τ_L ~120 ns, FWHM) or a wavelength-tunable OPO (Mirage 3000B, Continuum, Santa Clara, CA; τ_L = 6 ns, [26]) were used for primary material ablation. Throughout the experiments, the OPO laser was tuned to the Er:YAG wavelength of 2.94 μm. The beam of the respective laser was focused onto the sample at an angle of incidence of 45°. The elliptical

focal spot sizes were about 120 μm times 160 μm in diameter for both lasers. Care was taken that the apex of the glycerol drop was irradiated throughout the experiments.

Post-Ionization

Three different IR-lasers were used for infrared post-ionization (IRPI): an Er:YAG laser of the same type as the one described above, but with a slightly longer pulse duration of ~150 ns (FWHM), the above OPO, or an Er:YSGG laser (SEO 1-2-3, Schwartz Electro Optics, Orlando, FL; λ = 2.79 μm, τ_L = 70 ns). The OPO and Er:YAG lasers were operated in TEM_{00} mode with a Gaussian beam intensity profile in the focal beam waist. The Er:YSGG laser had a near-Gaussian beam profile in the focal beam waist. All three lasers emit with a near-Gaussian temporal pulse profile, as was measured with a fast IR-sensitive HgCdTe photodiode of ~1.5 ns time resolution.

The respective IRPI laser beam was aligned parallel to the plane of the sample plate. For all three lasers, the beam was focused with an infrasil lens (lens 1; Figure 1b) of 300 mm focal length, mounted outside the vacuum chamber. In case of the Er:YAG and the OPO laser, a two lens telescope (lenses 2 and 3; Figure 1b) was used to expand the beam by a ratio of 4:1 before final focusing in order to reduce the beam divergence. The focal beam waist diameters of the individual IRPI lasers were measured using thermo-sensitive paper as described previously [26]. They were ~80 μm for the Er:YAG and the OPO laser; the beam waist of the Er:YSGG laser was ~270 μm in diameter.

An xyz-micrometer translation stage was used to adjust the final focusing lens for IRPI beam steering with an accuracy of 5 μm. Care was taken to adjust the beam such that its beam waist was in front of the primary laser desorption spot. The zero position in the direction of the ion optical axis (z-direction) was defined by first moving the IRPI laser beam, i.e., the focusing lens, towards the droplet surface in z-direction until single-laser MALDI ion signals were generated while the primary desorption laser was blocked. At this distance, "shock waves" in the glycerol droplet were observed via the CCD camera, as a result of rapid heating and generation of pressure pulses [27]. The IRPI beam was then moved back gradually until no shock wave signals were visible anymore. The direct IR-MALDI ion signals consistently ceased at a beam position only a little closer to the target. The reproducibility of this procedure in defining the zero position was found to be about $\pm$10 μm.

Timing of the lasers and the oscilloscope was controlled by custom-built timing electronics. Two synchronized pulses drove the flash lamps of the two involved lasers with repetition rates of 10 Hz (OPO), 2 Hz (Er:YAG), and 1 Hz (Er:YSGG), chosen in order to achieve stable laser emissions and an integer ratio between the laser repetition rates. An operator-controlled switch triggers the emissions of the desorption laser by enabling the Q-switch. The trigger-circuits allow a continuous variation of the delay time between the desorption and the post-ionization laser pulses. For a given setting, the shot-to-shot variation in the delay was measured to be less than 100 ns. The exact time difference between the two laser pulses was monitored simultaneously with each recorded single-shot mass spectrum using pyroelectric sensors (model 420, Eltec Instruments, Daytona Beach, FL) for the Er:YAG and the Er:YSGG laser and the fast IR-photodiode for the OPO. The output of these sensors was monitored using a second oscilloscope (LeCroy 9350A, LeCroy, Chestnut Ridge, NY).

Laser fluences were adjusted with dielectric attenuators. Fluences were calculated by measuring the attenuated laser pulse energy with a high-precision energy meter (RK3230/337, Laser Precision Corp., Yorkville, NY) and dividing this value by the laser focal size. Transmission losses at lens and vacuum window surfaces were taken into account. The shot-to-shot pulse energy stability was approximately 2.5% for the OPO, 5% for the Er:YAG lasers, and 8% for the Er:YSGG laser (standard deviations).

For all measurements, the fluence of the primary laser was kept below the ion detection threshold H_0 for conventional, single-laser MALDI-MS. In case of the Er:YAG as primary laser, about 4500 J m^{-2} were applied with glycerol as matrix (H_0 ~5000 J m^{-2}); in case of the OPO as primary laser, 2500 J m^{-2} were applied (H_0 ~2700 J m^{-2}).

Blocking of either of the two (primary laser or postionization) beams proved that neither one generated ions in a conventional MALDI process. MALDI ion signals could be generated with the secondary laser on its own if this beam was adjusted to hit the glycerol drop surface at glancing angle.

The IRPI fluences in the beam waist, i.e., also in the region of interaction with the particle plume, were about 10,000 to a few 10,000 Jm^{-2} and were adjusted for either optimal ion signal (Figures 2, 3, 4) or for an optimal utilization of the dynamic range (Figures 5, 6, 7).

Materials

Glycerol (*p.a.*) was purchased from Fluka (Deisenhofen, Germany), angiotensin I and cytochrome *c* from Sigma (Schnelldorf, Germany), and the monoclonal antibody (IgG) from Eurogentec (Serain, Belgium). 20 mer DNA was purchased from Interactiva (Ulm, Germany) and 430 bp PCR-product DNA prepared in-house. All analytes were dissolved in bi-distilled water containing 0.1% TFA. Analyte/matrix samples were prepared on the sample plate by mixing ~1 μl analyte solution with ~1 μl glycerol. Most of the water content in the preparation was subsequently gassed off for some minutes in the rough vacuum of the sample transfer chamber (p ~10^{-2} mbar). Before final transfer, sample plates were dipped into liquid nitrogen for about 10 s, in order to

reduce glycerol evaporation in the high-vacuum of the mass spectrometer. The sample temperature upon transfer of the probe into the spectrometer was some minus ten degrees Celsius. The initial molar analyte-to-matrix (A/M) ratio was about 10^{-4}. Because samples warmed up with time, matrix evaporation was not entirely suppressed and molar A/M ratios approximately doubled within an hour. Care was taken to readjust both laser beams regularly to compensate for the receding droplet surface.

For water ice matrix preparations, cytochrome *c* was dissolved in bi-distilled water to $\sim 10^{-3}$ M. 1 μl of the solution was applied to the sample plate. Samples were cooled by dipping the plate into liquid nitrogen and rapidly transferred into the mass spectrometer.

Results and Discussion

Peptides and Proteins

Figure 2 displays three representative IRPI-MALD mass spectra of (2a) angiotensin I (1296.5 u), (2b) cytochrome *c* (horse heart; 12360 u), and (2c) of a monoclonal antibody (IgG; $\sim 150 \times 10^3$ u), respectively. All spectra were generated using glycerol as matrix. The mass spectra plotted in (2a) and (2c) were obtained with the Er:YAG as primary and the Er:YSGG as post-ionization laser. Figure 2b shows an example for the Er:YAG/OPO combination. Qualitatively, the spectra looked very similar for all laser combinations, including the combination of OPO/Er:YAG and that of two identical Er:YAG-lasers (data not shown). However, only cytochrome *c* as sample has been extensively tested with the four laser combinations so far. A significant quantitative difference was seen, if the Er:YSGG laser was used for IRPI. In this case, mass spectra could generally be recorded for substantially larger distances Δz of the IRPI laser beam from the glycerol drop surface and delay times τ_{IRPI} between the laser pulses. Mass spectra could for instance easily be recorded with the Er:YSGG IRPI-beam at distances Δz as large as 2.5 mm, whereas, if the Er:YAG or the OPO were employed, ion signals were generally found to cease well below a Δz of 0.5 mm (cf. Figure 7). Reasons for this different behavior could be the higher optical gas phase absorption of glycerol at 2.79 μm as compared to 2.94 μm [28], possibly allowing ionization also from a very thin plume. The higher available pulse energy of the Er:YSGG laser and larger interaction volume (beam waist diameter) could also contribute to this observation.

Elevation of the fluence of the desorption laser beam was found to enhance the IRPI ion yield strongly. However, for fluences above the conventional MALDI ion detection threshold, interpretation of the mass spectra gets rather complicated since each time-of-flight spectrum then consists of two superimposed, time-shifted spectra, one resulting from the conventional MALDI process and the other from IRPI. Separation of the two ion species proved to be difficult. Reduction of the ion mirror (reflector) voltage of the time-of-flight instrument to values below the nominal acceleration potential suppressed the primary ion signal to a large extent, but ion signals due to the decay of molecular ions and charged clusters were still found to distort the mass spectra considerably. Therefore, only primary laser fluences slightly below the conventional IR-MALDI ion detection threshold were applied in the experiments.

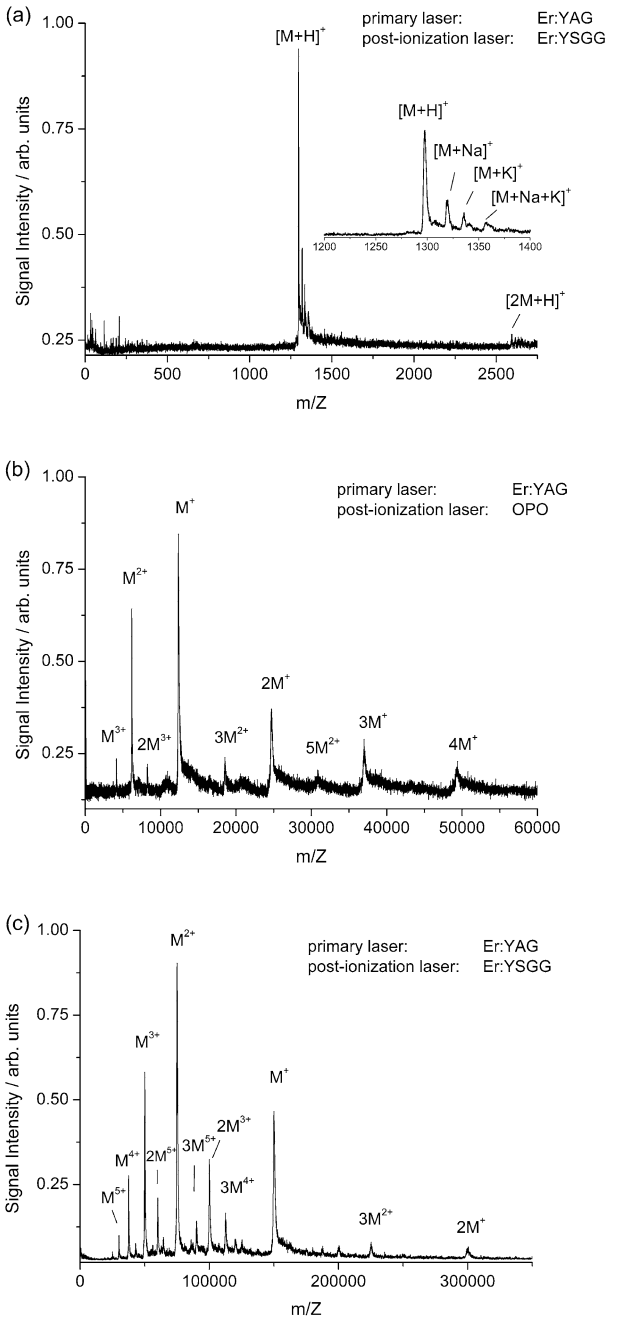

Figure 2. IRPI-MALD mass spectra of (**a**) angiotensin I (1296.5 u; $\Delta z \sim 0.5$ mm; $\tau_{IRPI} \sim 1.8$ μs (in this case, delayed ion extraction was used in order to improve peak resolution), (**b**) cytochrome *c* (12360 u; $\Delta z = 100$ μm; $\tau_{IRPI} = 1.5$ μs), and (**c**) monoclonal antibody (IgG; $\sim 150 \times 10^3$ u; $\Delta z \sim 1.0$ mm; $\tau_{IRPI} = 2.0$ μs). Primary laser: Er:YAG; IRPI laser: (**a**) and (**c**) Er:YSGG, (**b**) OPO; matrix: glycerol. Sum of 30 single-shot mass spectra each.

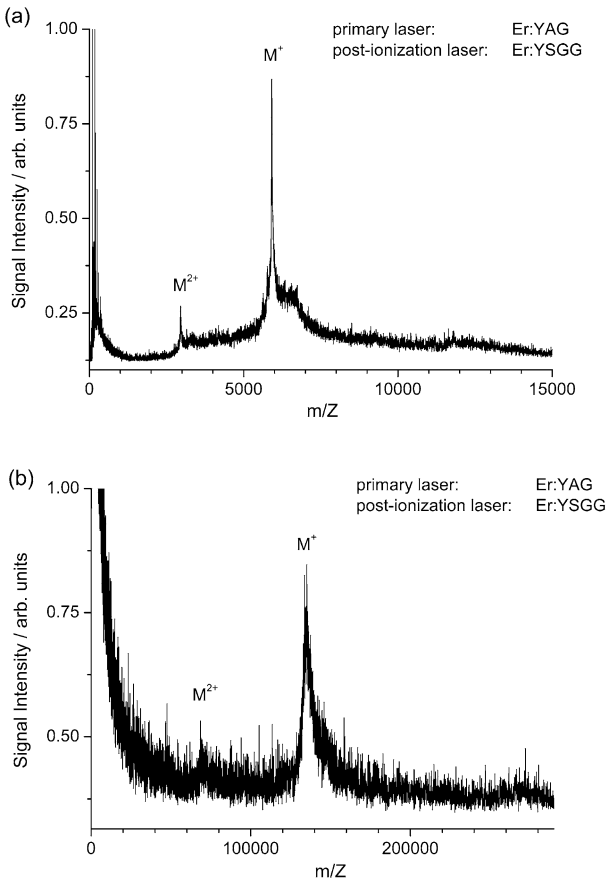

Figure 3. IRPI-MALD mass spectra of (**a**) 20mer DNA (6117 u; Δz = 1.0 mm; τ_{IRPI} = 2.0 μs) and (**b**) 430 mer DNA (133 $\times$ 10^3 u ; Δz = 1.0 mm; τ_{IRPI} = 2.0 μs). Primary laser: Er:YAG; IRPI laser: Er:YSGG; matrix: glycerol. Sum of (**a**) 85 and (**b**) 60 single-shot mass spectra.

The analytical sensitivity in terms of the minimal necessary sample amount has not been tested explicitly so far. For peptides and proteins the ion signal strength and S/N ratio was comparable to that of the direct IR-MALDI signals recorded with the same instrument (see also [29]). The maximun FWHM mass resolution was about 400 for peptides (using delayed ion extraction, Figure 2a) and about 100 for proteins. For the detection of the angiotensin I ions, delayed ion extraction was used. All other mass spectra were obtained with continuous ion extraction. In comparison, direct IR-MALDI mass spectra of small peptides, recorded with the same instrument and delayed ion extraction, have a FWHM mass resolution of up to 3000. A combination of the IRPI ion source with mass analyzers, which decouple ionization and detection in a stronger manner, like o-TOF instruments, may considerably improve the performance.

Nucleic Acids

IRPI-MALD mass spectra of a single-stranded 20 mer (6117 u) and a double-stranded 430 mer DNA (mass of the single strand, 133 $\times$ 10^3 u) are displayed in Figure 3a and b, respectively. All DNA ions were detected in form of single-stranded molecules. For the DNA samples, the quality of the mass spectra was lower than that achieved by direct IR-MALDI-MS [30].

Water Ice as Matrix

Figure 4 demonstrates that IRPI mass spectra of large biomolecules can also be produced from other than the glycerol matrix. In this case, cytochrome *c* ions were generated from a water ice matrix. Compared to the mass spectra obtained with glycerol, the ion distribution is notably shifted to higher charge states, in line with previous observations in which water ice was used in direct IR-MALDI experiments [31]. IRPI-MALD mass spectra and conventional IR-MALDI-MS spectra acquired from the same sample were qualitatively comparable, though the overall signal intensity was substantially lower for IRPI.

Mechanisms of IRPI

Given the low photon energies of 0.44 eV at λ = 2.79 μm and 0.42 eV at λ = 2.94 μm, and the relatively low applied PI laser fluences of ~10,000 J m^{-2}, corresponding to irradiances of ~10^7 W cm^{-2} for a 100 ns pulse, multiphoton ionization of single molecules does not seem to be a likely and therefore relevant process. Also the strong dependence of the ion yield on the size of the biomolecules, as observed in UV-REMPI-MS speaks against such a mechanism [10]. Therefore, ions must be assumed to be generated essentially from small analyte-matrix droplets/clusters in a secondary laser-induced matrix-assisted desorption/ionization step. In fact, at least for peptides proteins, normal IR-MALDI and the IRPI results look very similar and a molecular size discrimination like in UV-REMPI was not notable.

Results from time-resolved fast-flash photography of the glycerol plume, recently carried out in our laboratory, provide further evidence for the ejection of a dense glycerol plume, consisting of a mixture of molecular vapor and droplets/clusters [32]. These results will be published in a separate article.

Plume Expansion Dynamics

The post-ionization method can also be used as a tool to investigate details of the MALD plume expansion.

Different experiments were performed: In the first one, the IRPI laser beam was positioned at a fixed distance Δz of ~0.5 mm. Angiotensin I mass spectra were recorded for different delay times τ_{IRPI} between the laser pulses. In this experiment, the Er:YAG laser was used for primary ablation and the Er:YSGG laser for IRPI. The results are plotted in Figure 5. Post-ionization signals commence in between 100 ns and 500 ns, indicating a fast "front velocity" of the plume on the order of 1000 ms^{-1}. The results also demonstrate a wide

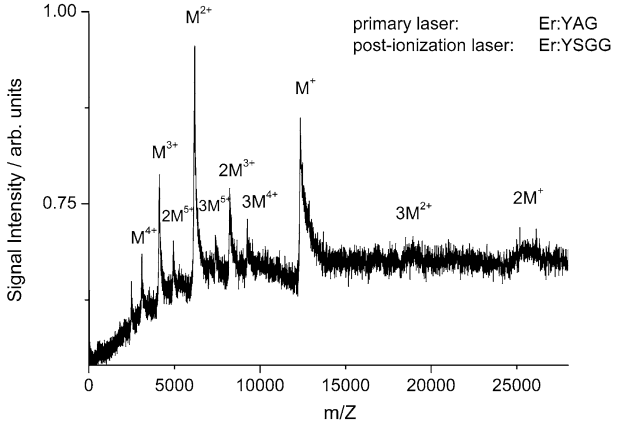

Figure 4. IRPI-MALD mass spectrum of cytochrome *c* (12360 u), acquired from a water ice matrix (molar A/M ratio, $\sim 10^{-3}$). Primary laser: Er:YAG; IRPI laser: Er:YSGG; Δz = 0.5 mm; τ_{IRPI} = 3.0 μs. Sum of 40 single-shot mass spectra.

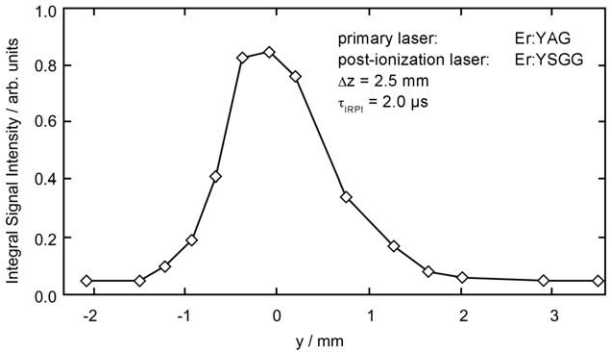

Figure 6. Signal intensity of singly-charged molecular cytochrome *c* ions as a function of the lateral (y−) position of the IRPI laser beam relative to the ion optical axis. Primary laser: Er:YAG; IRPI laser: Er:YSGG; matrix: glycerol; $\Delta z \sim 2.5$ mm; τ_{IRPI} = 2.0 μs. For each data point, 10 single laser shot mass spectra were summed.

energy distribution of the plume. IRPI ion signals, probably originating from residual droplets, were even detected at delay times exceeding 50 μs. With different methods, the mean axial velocities of IR-MALDI ions, also generated from a glycerol matrix, have recently been investigated [34]. The average value of ~1000 ms^{-2} as determined in that study suggests that ions are essentially part of a fast "gaseous" part of the plume, not fully registered by IRPI.

In the second experiment, the delay time between the laser pulses was fixed to τ_{IRPI} = 2.0 μs, the axial position Δz was fixed to 2.5 mm, and the IRPI beam was scanned in the direction perpendicular to the ion optical axis. Signal intensities of singly-charged molecular cytochrome *c* ions were recorded as a function of this lateral (y−) position. The results of this experiment are plotted in Figure 6. These data reveal a large angle of expansion of the propagating plume. At ~40° full opening angle, the ion signal drops to 1/e of the maximum at 0° (y = 0). Signals of small but significant intensity are even recorded up to 72°.

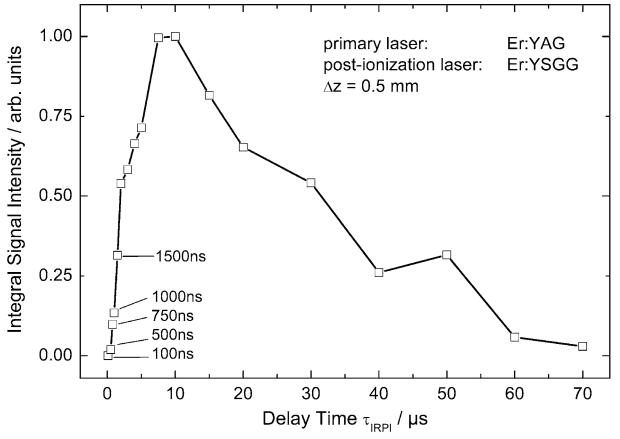

Figure 5. Signal intensity of singly-charged molecular angiotensin I ions as a function of delay time τ_{IRPI} between the two laser pulses. Primary laser: Er:YAG; IRPI laser: Er:YSGG; $\Delta z \sim 0.5$ mm; matrix: glycerol. For each data point, 50 single laser shot mass spectra were summed.

In a third set of experiments, shorter distances Δz, close to the glycerol drop, were chosen, in order to follow the initial phase of the plume expansion, and in particular, to investigate the previously observed strong effect of the laser pulse duration on the IR-MALDI process [27, 34] in more detail. The OPO and the Er:YAG laser with their pulse durations of 6 ns and 120 ns, respectively, were compared as primary desorption laser source.

Figure 7 displays the signal intensities of singly-charged molecular cytochrome *c* ions as a function of Δz and τ_{IRPI}. Data points were binned for time windows of 10 and 20% of the delay time for small and large delay times, respectively. In Figure 7a, the OPO (τ_L= 6 ns) was used as primary laser and one of the two available Er:YAG lasers (τ_L= 150 ns) was used for IRPI; in 7b, the other Er:YAG (τ_L= 120 ns) was used as primary laser and the OPO for IRPI.

If the OPO is used as desorption laser, the maximum signal intensity is obtained at the shortest distances and delay times. For small τ_{IRPI} values, a monotonic decrease with Δz is observed. For delay times above about 1 μs, the center-of-mass motion of the plume becomes visible and leads to a peaked intensity of the 1500 ns profile at a Δz of about 50 μm.

In contrast, material ejection after Er:YAG excitation appears considerably prolonged (Figure 7b). Here, signal intensities are rather low for short delay times τ_{IRPI} and distances Δz but increase substantially with delay time. For a delay time of 1.5 μs, the maximum signal intensity is obtained, at a distance Δz in between 30 and 50 μm.

Figure 7c displays the intensity-delay time profile for a fixed distance Δz of 40 μm obtained for the Er:YAG/OPO combination. At this distance, ion signals rise very sharply with τ_{IRPI} until a maximum is reached at a delay of about 2 μs. Ion signals of small intensities could be recorded for delay times as long as 30 μs. In contrast,

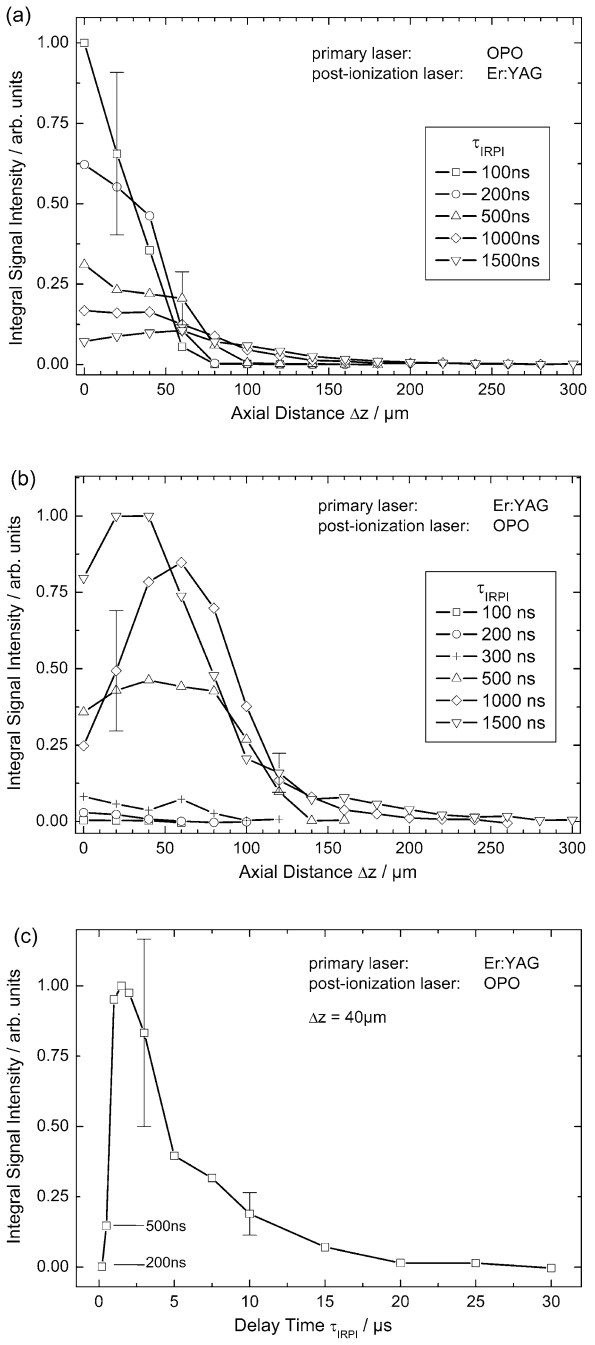

Figure 7. Signal intensity of singly-charged molecular cytochrome *c* ions as a function of the axial distance Δz of the IRPI laser beam relative to the apex of the glycerol drop, i.e., the primary laser spot, and the delay time τ_{IRPI} between the laser pulses. Matrix: glycerol. (**a**) Primary laser: OPO; IRPI laser: Er:YAG. (**b**) Primary laser: Er:YAG; IRPI laser: OPO. (**c**) Same measurement as in (**b**) with a fixed distance Δz of 40 μm and longer applied delay times τ_{IRPI}. The primary laser fluence was in all three cases slightly below the ion detection threshold for conventional single-laser IR-MALDI-MS, i.e., ~2400 J m^{-2} for the OPO and ~4500 J m^{-2} for the Er:YAG as primary laser. For each data point, 30 single laser shot mass spectra were summed.

IRPI signals ceased substantially earlier for the OPO/Er:YAG combination.

Assuming that the different post-ionization laser pulse widths do not influence the relative spatial-temporal PI yield substantially, a clear dependence of the plume dynamics on the pulse duration of the primary desorption laser would be derived. The results also suggest that a temporal and geometrical size distribution of clusters or droplets exists, from which a fraction is at optimum for post-ionization.

These post-ionization results correspond well to those from a recent study, in which the time-resolved rate of material ejection was measured with a photoacoustic sensor, registering the recoil momentum of ablated material as a function of laser fluence and pulse duration [27], and with those obtained with fast flash photography [32]. In both studies, an instantaneous ejection was indicated for the OPO, in contrast to prolonged material ejection for the Er:YAG.

Conclusions

This article introduces a novel method for the generation of large biomolecular ions. The two IR-laser approach can potentially offer some advantages. For example, In comparison to LILBID-MS, sample consumption is reduced by several orders of magnitude. The accessible mass range is larger by two orders of magnitude than that previously realized by REMPI with UV-lasers and is probably very similar to that of conventional IR-MALDI-MS.

Because primary vaporization and secondary desorption/ionization are decoupled, IRPI may potentially be applied to materials and conditions which are not amenable to single-laser MALDI-MS. This may also allow to overcome current limitations of MALDI with very small spot sizes in the micron range, for which larger peptides and proteins can not be detected as intact molecular ions [35]. Further studies with solid state matrices are, therefore, clearly desirable. The primary infrared laser can probably be straightforwardly substituted with a pulsed UV-laser if laser wavelength and optical absorption of the matrix are chosen suitable to produce droplets/particles of the right size distribution for IRPI. For many samples, the first laser may also not constitute a principle prerequisite. In fact, a highly interesting application would be the use of the IR-laser for ionization in aerosol mass spectrometry, potentially allowing to generate (intact) biomolecular ions of high significance.

Acknowledgments

The authors thank M. Schürenberg for his input in the brainstorming stage of this project and U. Röhling for development of the delay time control. AR gratefully acknowledges financial support by a Ph.D. grant from the University of Münster. This work was done in partial fulfillment of the requirements for the Ph.D. of AL and AR at the University of Münster.

References

1. Karas, M.; Bachmann, D.; Bahr, U.; Hillenkamp, F. *Int. J. Mass Spectrom. Ion Processes* **1987,** *78,* 53.
2. Karas, M.; Hillenkamp, F. *Anal. Chem.* **1988,** *60,* 2299.
3. Dreisewerd, K. *Chem. Rev.* **2003,** *103,* 395.
4. Dreisewerd, K.; Berkenkamp, S.; Leisner, A.; Rohlfing, A.; Menzel, C. *Int. J. Mass Spectrom.* **2003,** *226,* 189.
5. Zenobi, R.; Knochenmuss, R. *Mass Spectrom. Rev.* **1998,** *17,* 337.
6. Beavis, R. C.; Chait, B. T. *Rapid Commun. Mass Spectrom.* **1989,** *3,* 233.
7. Overberg, A.; Karas, M.; Bahr, U.; Kaufmann, R.; Hillenkamp, F. *Rapid Commun. Mass Spectrom.* **1990,** *4,* 293.
8. Overberg, A.; Karas, M.; Hillenkamp, F. *Rapid Commun. Mass Spectrom.* **1991,** *5,* 128.
9. Boesl, U.; Weinkauf, R.; Weickhardt, C.; Schlag, E. W. *Int. J. Mass Spectrom. Ion Processes* **1994,** *131,* 87, and references therein.
10. Schlag, E. W.; Grotemeyer, J.; Levine, R. D. *Chem. Phys. Lett.* **1992,** *190,* 521.
11. Morris, G. B.; Johnston, J. *J. Phys. Chem.* **1985,** *89,* 5399.
12. Rizzo, T. R.; Park, Y. D.; Petenau, L. A.; Levy, D. H. *J. Chem. Phys.* **1985,** *83,* 4990.
13. Von Helden, G.; Van Heijnsbergen, D.; Mejer, G. *J. Phys. Chem. A* **2003,** *107,* 1671.
14. Little, M. W.; Kim, J. K.; Murray, K. K. *J. Mass Spectrom.* **2003,** *38,* 772.
15. Noble, C. A.; Prather, K. A. *Mass Spectrom. Rev.* **2000,** *19,* 248.
16. Johnston, M. V. *J. Mass Spectrom.* **2000,** *35,* 585.
17. Murphy, D. M.; Thomson, D. S. *Aerosol Sci. Res.* **1995,** *22,* 237.
18. Hinz, K.-P.; Kaufmann, R.; Spengler, B. *Anal. Chem.* **1994,** *66,* 2071.
19. He, L.; Murray, K. K. *J. Mass Spectrom.* **1999,** *34,* 909.
20. Thomson, D. S.; Murphy, D. M. *Appl. Opt.* **1993,** *32,* 6818.
21. Dessiaterik, Y.; Nguyen, T.; Baer, T.; Miller, R. E. *J. Phys. Chem. A* **2003,** *107,* 11245.
22. Kleinekofort, W.; Avdiev, J.; Brutschy, B. *Int. J. Mass Spectrom. Ion Processes* **1996,** *152,* 135.
23. Wattenberg, A.; Sobott, F.; Brutschy, B. *Rapid Commun. Mass Spectrom.* **2000,** *14,* 859.
24. Wattenberg, A.; Sobott, F.; Barth, H. D.; Brutschy, B. *Int. J. Mass Spectrom.* **2000,** *203,* 49.
25. Hiraoka, K.; Saito, S.; Katsurawa, J.; Kudaka, I. *Rapid Commun. Mass Spectrom.* **1998,** *12,* 1170.
26. Menzel, C.; Dreisewerd, K.; Berkenkamp, S.; Hillenkamp, F. *Int. J. Mass Spectrom.* **2001,** *207,* 73.
27. Rohlfing, A.; Menzel, C.; Kukreja, L. M.; Hillenkamp, F.; Dreisewerd, K. *J. Phys. Chem. B* **2003,** *107,* 12275.
28. NIST Chemistry WebBook (http://webbook.nist.gov/chemistry).
29. Berkenkamp, S.; Menzel, C.; Karas, M.; Hillenkamp, F. *Rapid Commun. Mass Spectrom.* **1997,** *11,* 1399.
30. Kirpekar, F.; Berkenkamp, S.; Hillenkamp, F. *Anal. Chem.* **1999,** *71,* 2334.
31. Berkenkamp, S.; Karas, M.; Hillenkamp, F. *Proc. Natl. Acad. Sci. U.S.A.* **1996,** *93,* 7003.
32. Leisner, A. Dissertation, University of Münster, 2004.
33. Berkenkamp, S.; Menzel, C.; Hillenkamp, F.; Dreisewerd, K. *J. Am. Soc. Mass Spectrom.* **2002,** *13,* 209.
34. Menzel, C.; Dreisewerd, K.; Berkenkamp, S.; Hillenkamp, F. *J. Am. Soc. Mass Spectrom.* **2002,** *13,* 975.
35. Spengler, B.; Huber, M. *J. Am. Soc. Mass Spectrom.* **2002,** *13,* 735.